TÜBİTAK

Turkish Journal of Physics

http://journals.tubitak.gov.tr/physics/

Research Article

Turk J Phys
(2018) 42: 659 – 667
© TÜBİTAK
doi:10.3906/fiz-1806-18

Isotopic distribution in projectile fragments above the Coulomb barrier

Ayşegül KAYA, Nihal BÜYÜKÇİZMECİ, Rıza OĞUL*
Department of Physics, Faculty of Science, Selçuk University, Konya, Turkey

Received: 21.06.2018 • **Accepted/Published Online:** 02.11.2018 • **Final Version:** 14.12.2018

Abstract: We have studied fragmentation properties of projectiles in peripheral heavy-ion collisions within a statistical ensemble approach. Distributions of projectile fragments are calculated for the reaction systems ^{86}Kr on ^{58,64}Ni and are compared to the experimental data for the same reactions at projectile energy of 15 MeV/nucleon. We assume that the projectile nuclei capture many neutrons from the targets as a result of the multinucleon transfer reactions (direct and fast reactions) at the first step of the dynamical stage of the collisions, and then the excited spectators are formed during the preequilibrium process (multistep reactions) long before the statistical equilibrium stage, and the deexcitation processes for the hot sources are simulated within the statistical multifragmentation model. It is seen that predicted results are in satisfactory agreement with experimental data.

Key words: Isotopic distribution, mass distribution, projectile fragment

1. Introduction

The properties of exotic nuclei close to the neutron dripline are important to provide information about the evolution of nuclear structure and nucleosynthesis [1,2]. They also provide us with crucial information for the simulation of astrophysical phenomena such as supernova explosions and neutron star dynamics [3,4]. The neutron-rich exotic nuclei are mainly produced in nuclear reactions between the projectile and target nuclei at various energies. There are many forms of classifications for these reactions according to the excitation or beam energy intervals. The main examples of such reactions are fission, fusion, nuclear fragmentation, and nucleon transfer reactions. Beside the low-energy fission reactions of heavy nuclei, neutron-rich nuclei are also produced by proton stripping in nuclear fragmentation reactions of relativistic heavy projectiles [5,6]. Another reaction channel where both neutron-rich and neutron-poor isotopes are produced is multinucleon transfer reaction, the so-called nucleosynthesis, with consecutive neutron or proton captures near the Coulomb barrier. At the low-energy region up to the Coulomb barrier, neutron-poor fragments are produced as a result of fusion reactions in central collisions of heavy nuclei. Recently, experimental and theoretical studies have demonstrated that the neutron-rich fragments are also produced in the deep inelastic transfer reactions occurring in the region between the Coulomb barrier and Fermi energy regime [7–9]. Starting from the Fermi energy regime up to relativistic energies, nuclear multifragmentation reactions become superior to produce neutron-rich and proton-rich fragments [10–12].

In this study, we investigate the applicability of the statistical multifragmentation model (SMM) [13] in the transition region between the Coulomb barrier and Fermi energy regime. Experimental data in Ref. [12]

*Correspondence: rogul@selcuk.edu.tr

show that multifragmentation reactions still take place at 15 MeV/nucleon in this transition region (see the scatter plots therein). Therefore, we used the SMM for the present calculations of fragment yields produced in ^{86}Kr $+^{58,64}$Ni reactions at 15 MeV/nucleon, too. Recently, we also successfully applied the SMM for the analyses of various experimental data [14–17] for similar reactions. For the present calculations, we consider the ensemble version of the SMM, and then we compare our predicted results with the experimental data obtained at the Cyclotron Institute of Texas A&M University (TAMU) [9,12].

In the next section, we shall briefly discuss the statistical model used in the present calculations to determine the characteristics of fragment mass and isotope distributions for the abovementioned reaction systems. We briefly discuss the simulation of the fragmentation mechanism of excited projectile sources within the statistical ensemble approach on the basis of the SMM with the results of the present calculations and comparison with the experimental data in Section 3. The present findings will also be related to our previous studies in a similar context. Finally, we give the conclusions and discussion in Section 4.

2. Statistical model

In the literature, there are various models to describe the nuclear multifragmentation mechanism according to the excitation energy deposited in projectile sources. In these models, if the excitation energy per nucleon is less than 1 MeV/nucleon, the decay modes are generally described by the collective modes of compound atomic nuclei. At higher energies, the fragment characteristics are described according to the statistical and other existing models [18–21]. The predicted results obtained in these models have been seen to be consistent with the experimental data [14–20]. In the simulation of the reaction processes, one generally describes an intermediate excited nucleus formation in the first stage, and in the second stage, a secondary excitation process (deexcitation) of excited sources is simulated with an evaporation code. In the present calculations ensemble formations of the excited fragments are simulated according to the SMM [22]. In the ensemble version of the SMM the multifragmentation process is subdivided into three stages: a dynamical stage (leading to the formation of an equilibrated ensemble of sources), the disassembly of the system into individual primary fragments, and the subsequent deexcitation of hot primary fragments. At the beginning of the dynamical stage (direct and fast stage), we consider multinucleon exchange reactions characterized by short reaction times of $\sim 10^{-22}$ s, and a preequilibrium process that takes place after the first stage but long before the statistical equilibrium is reached at low density freeze-out (formation of ensemble of hot sources). The deexcitation process leading to the formation of cold fragments starts after the disassembly of the system into the primary hot fragments. There is another concern about the formation of the excited spectators, namely whether sufficient excitation energy is accumulated in the projectiles for the multifragmentation at 15 MeV/nucleon. Universality of the excitation energy, which implies that the excitation energy of the spectators is not very dependent on the projectile energy, was shown in the analyses of the experiments. The limitation of the excitation energy is due to the preequilibrium emissions at the dynamical stage (for details, see Ref. [22]). At the final stage of the multifragmentation reactions, the deexcitations of hot fragments are simulated according to the SMM code. In the present approach, we assume that fragmentation channels consist of neutrons and protons, and the conservations of the number of particles, energy, and angular momentum in each step of the calculations are taken into account. Beside multifragmentation channels, the compound-nucleus channels, conventional evaporation, and fission channels, as well as the transition region between the low- and high-energy deexcitation regimes, are also included in the SMM code. The competition between all channels is permitted in the code. Here we should point out that one may also define the SMM in terms of clusterization of the fragments in the

thermodynamic limit. In this case, the fragments composed of protons and neutrons are considered as liquid drops of the nuclear phases [23,24]. In the microcanonical limit, one may define the weight of the fragmentation probability of each event as follows:

$$\xi W_j = exp(S_j\,(E^*, A, Z) \tag{1}$$

Here, ξ the normalization constant, S_j is the entropy of each channel, E^* is the excitation energy, A is the mass number, and Z is the charge number of the droplets. The decay channels are generated by the Monte Carlo method according to their statistical weights. Light fragments with mass number $A \leq 4$ and charge number $Z \leq 2$ are considered as nuclear gas of elementary particles, and the other ones are called fragments (liquid phase). The free energy of a fragmentation channel can be defined in terms of the parameters of the Bethe–Weizsacker formula as a sum of the bulk, surface, Coulomb, and symmetry energy terms as

$$F_{A,Z} = F^B_{A,Z} + F^S_{A,Z} + F^C_{A,Z} + F^{sym}_{A,Z} \tag{2}$$

Here, $F^B_{A,Z} = (-W_0 - T^2/\varepsilon_0)A$ is the bulk term (with temperature T, level density parameter ε_0, and binding energy $W_0 = 16$ MeV for symmetric nuclear matter), $F^S_{A,Z} = B_0 A^{2/3}[(T_c^2 - T^2)/(T_c^2 + T^2)]^{5/4}$ is the surface energy (with surface energy term $B_0 = 18$ MeV, and critical temperature $T_c = 18$ MeV), $E^C_{A,Z} = (cZ^2)/A^{1/3}$ is the Coulomb energy contribution (with the Coulomb parameter c obtained in Wigner–Seitz approximation as $c = (3/5)\ (e^2/r_0 - (\rho/\rho_0)^{1/3})$, charge unit $e, r_0 = 1.17$ fm, normal nuclear matter density $\rho_0 = 0.15\ fm^{-3}$), and $E^{sym}_{A,Z} = \gamma(A - 2Z)^2/A$ as the symmetry term (with the ground state value of the symmetry energy parameter $\gamma = 25$ MeV). These parameters are defined according to the Bethe–Weizsacker formula for the ground state values of isolated fragments at saturation density. In the low-density freeze-out region one may consider the modifications of liquid-drop parameters through the analyses of experimental data. In the present calculations we use the statistical ensemble approach to simulate the reaction processes. In one of our previous studies, we fully described this procedure in terms of excitation energy as a function of mass of the excited fragments of ensemble of sources [14].

2.1. Secondary excitations of hot fragments

In this section, we summarize the main secondary excitation (deexcitation) processes for the primary hot fragments. For excitation energies $E^* \leq 1$ MeV/nucleon, the secondary excitation of the hot particles can be simulated according to the SMM code within the standard Weisskopf evaporation and fission scheme [25]. The decay of light fragments $A \leq 16$ can be described by the Fermi break-up model. In the microcanonical approximation we take into account all possible breakup channels satisfying the conservation of energy, momentum, and particle numbers A and Z. We assume that the probability of each event channel is proportional to the occupied states in the phase space. The weight of the channels containing n particles with masses mi $(i = 1, ..., n)$ is given by

$$\Delta\Gamma^{mic}_f \propto \frac{S}{G}\left(\frac{V_f}{(2\pi\eta)^3}\right)^{n-1}\left(\frac{\prod_{i=1}^n m_i}{m_0}\right)^{\frac{3}{2}}\frac{(2\pi)^{\left(\frac{3}{2}\right)(n-1)}}{\Gamma\left(\frac{3}{2}(n-1)\right)}\left(E_{kin} - U^C_f\right)^{\left(\frac{3}{2}\right)n-\frac{5}{2}}, \tag{3}$$

where $m_0 = \sum_{i=1}^n m_i$ is the total mass, $S = \Pi_{i=1}^n (2s_i + 1)$ is the spin degeneracy factor, $G = \Pi_{j=1}^k n_j!$ is the particle identity factor with n_j the number of the jth particles, E_{kin} is the total kinetic energy of the fragments,

and U_f^C is the Coulomb interaction energy of secondary cold particles. The total excitation energy E* can be expressed using the conservation of total energy.

Sequential decay modes of primary hot fragments with mass number A >16 were studied nearly 60 years ago as excited modes of compound nuclei [25]. This mechanism has been investigated extensively, and it was shown that compound nucleus models successfully reproduce the experimental data [13]. The emission width of a particle j emitted from the compound nucleus (A, Z) is given by

$$\Gamma_j = \sum_{i=1}^{n} \int_0^{E^*_{AZ}-B_j-\varepsilon_j^{(i)}} \frac{\mu_j g_j^{(i)}}{\pi^2 \eta^3} \sigma_j(E) \quad \frac{\rho_{A'Z'}(E^*_{AZ} - B_j - E)}{\rho_{AZ}(E^*_{AZ})} E dE, \tag{4}$$

where the summation is taken over all the states (ground and excited states), $\varepsilon_j^i (i = 0, 1, ..., n)$ is for the fragments $j, g_j^{(i)} = (2s^{(i)}j + 1)$ is the spin degeneracy factor of the excited state $j, \mu j$ is the reduced mass, Bj is the separation energy, $E^*_{A,Z}$ is the excitation energy of the source, and E is the kinetic energy of an emitted particle in the center-of-mass frame. In this equation, ρ_{AZ} and $\rho_{A'Z'}$ correspond to the initial and final level densities in the evaporation chain. The cross-section $\sigma_j(E)$ of the inverse reaction $(A', Z') + j = (A, Z)$ is obtained from the optical model calculations by using the same potential defined in Ref. [26]. The Monte Carlo method is used to simulate this process by considering the conservation of energy and momentum for each emission step. It is concluded that if the excitation energy is more than 1 MeV/nucleon, one should consider the fact that the symmetry energy coefficient in the mass formula tends to decrease. In this way, one may obtain a suitable description for the isotopic distributions [27–31]. For the excitations ($E^* > 2$ MeV/nucleon) multifragmentation reactions are dominant compared to the other channels such as evaporation and fission, and at lower energies ($E^* \leq 2$ MeV/nucleon) the intermediate and heavy isotopes (A > 16) show particle evaporation in addition to fission reactions, for which the Bohr–Wheeler statistical approach is assumed [13]. In this approach, it is assumed that the partial width is proportional to the level density at the saddle point for the fission of the excited compound nucleus. In this case, the height of the fission barrier is determined by the Myers–Swiatecki model. The shell effects are negligible in determination of the level densities, since a broad range of distribution of excitation energy is considered.

3. Mass and isotopic distributions of fragments

The measured production cross-sections for the projectile fragments in the reactions ^{86}Kr $+^{64}$Ni and ^{86}Kr $+^{58}$Ni at 15 MeV per nucleon were given in [9,12]. In our theoretical simulation of the same reactions, it is assumed that neutron-rich ^{90}Kr and ^{92}Kr quasiprojectiles are formed in the dynamical stage of the collisions as predicted by the deep inelastic transfer (DIT) model [12]. According to the DIT model, at the beginning of the nuclear reactions, neutron capture processes are described to compose the quasiprojectiles (up to 4–8 neutrons). In the present study, disintegration of the excited sources into hot fragments and the secondary excitations of the hot fragments are described within the SMM code. Assuming the quasiprojectiles ^{90}Kr and ^{92}Kr are formed at the initial stage of the reactions, respectively, we have simulated the fragmentation of these excited sources to obtain the present results. We observed a satisfactory agreement between the data given in Ref. [9,12] and our results obtained within the SMM. As expected, we also demonstrated that neutron-rich sources provide more neutron-rich fragment production in the reactions near Coulomb barriers. During this kind of reactions, the excitation energy deposited in the sources may drop below the particle evaporation threshold. In

this case, one should consider the Weisskopf evaporation scheme to take into account the secondary excitation of hot fragments in the SMM code.

Figure 1 shows the results obtained from the present calculations for the distributions of the primary hot and final cold fragments produced within the SMM ensemble version. The upper panel shows the average multiplicity of hot and cold fragments from the ensemble of sources of ^{90}Kr and the lower panel for the more neutron-rich ^{92}Kr. The difference between hot and cold distributions is simply due to the fact that the mass of a hot fragment is reduced after the particle emission in deexcitation process. It is also seen that neutron-rich sources produce neutron-rich fragments, which is in agreement with our previous findings [14–17]. In the present study, the calculations were performed for 500,000 iterations, and we consider the ALADIN parameters determined in Ref. [14] for relativistic collisions. We recently showed that the ensemble approach can be applied to reproduce the experimental data for intermediate energy nuclear collisions, too [32]. This is because the universality characteristic of the excitation energy deposition holds in a wide range of energy regimes.

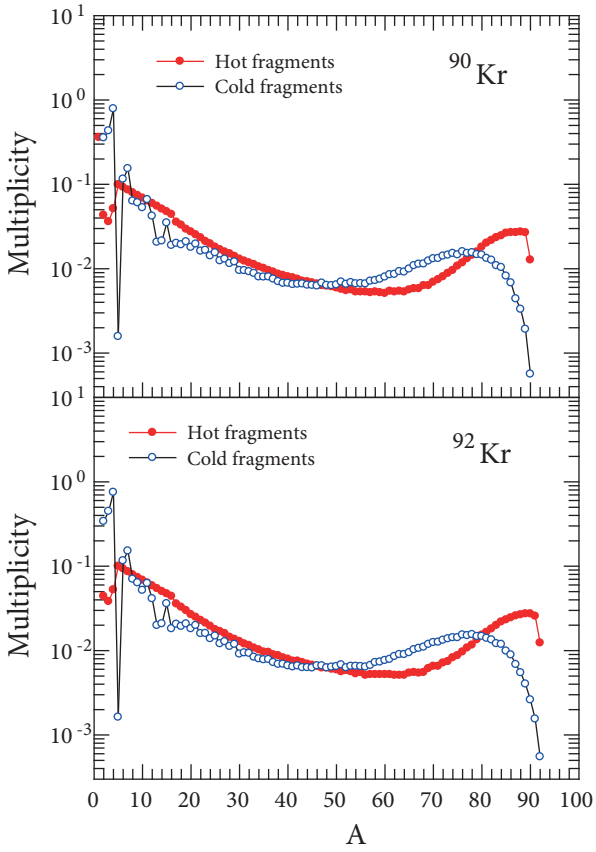

Figure 1. Theoretically predicted mass distributions of primary hot (red solid circles) and secondary cold fragments (blue empty circles) produced from the ensemble sources for ^{90}Kr and ^{92}Kr quasiprojectiles assumed to be formed through the deep inelastic neutron transfer in the reactions ^{86}Kr + ^{58}Ni and ^{86}Kr + ^{64}Ni at 15 MeV/nucleon, respectively.

In Figure 2, we compare our predicted production cross-section values for the near-projectile fragments with Z = 30–35 (dashed and solid lines) with the experimental data measured at TAMU (full and empty circle). We have carried out the normalizations of obtained results according to the experimental cross-sections. The resulting values for the normalization factors are 0.0017, 0.0012, 0.0013, 0.0020, 0.0044, and 0.015 mb per

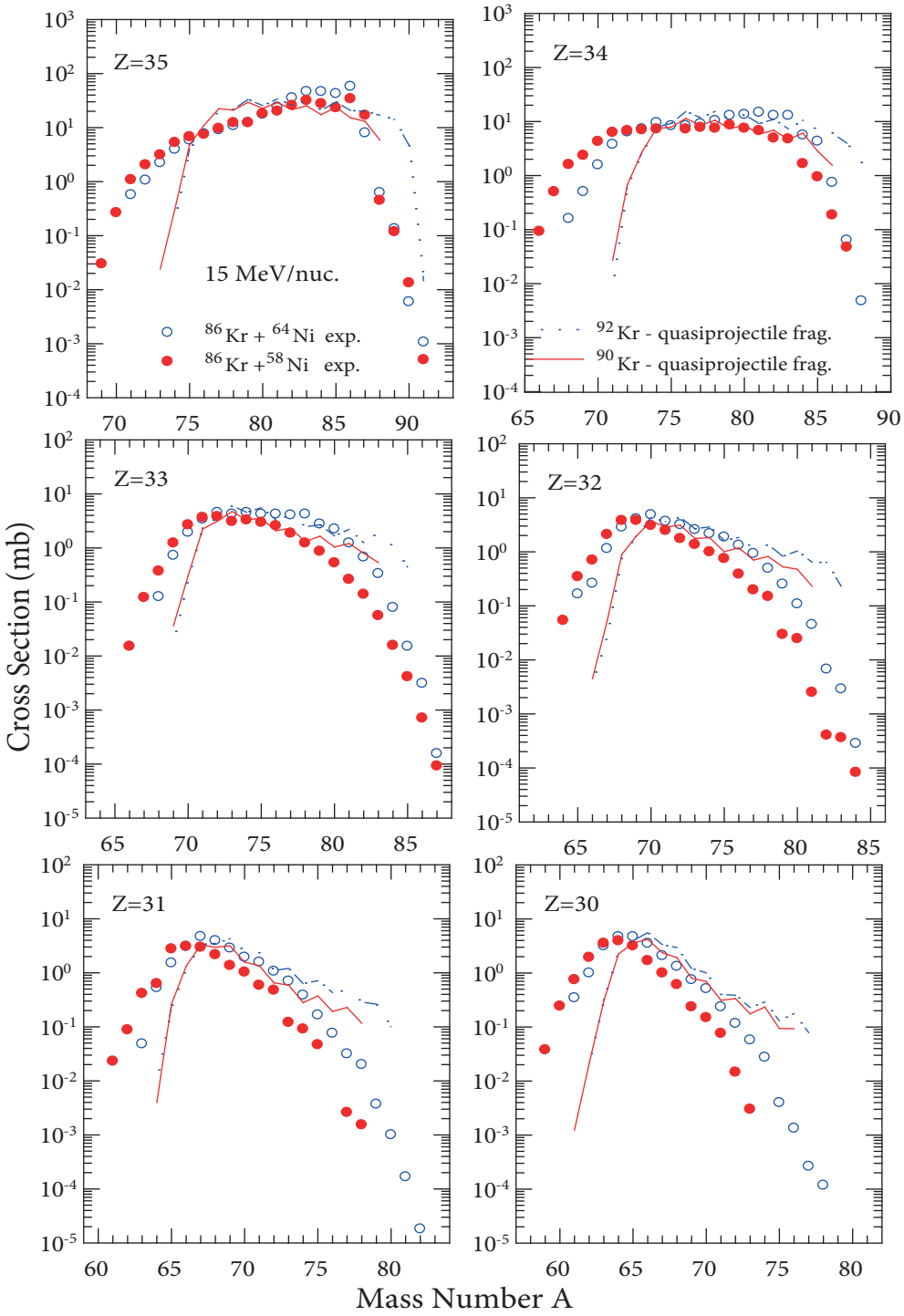

Figure 2. Isotopic distributions of near-projectile fragments produced from the ensemble sources for ^{90}Kr and ^{92}Kr quasiprojectiles assumed to be formed through the deep inelastic neutron transfer in the reactions ^{86}Kr +^{58}Ni and ^{86}Kr + ^{64}Ni at 15 MeV/nucleon, respectively. Solid and dashed lines show the results of our calculations, and the circles show experimental data for each reaction system. The colors are defined for each reaction as shown in the top panels.

theoretical event for the fragments of ^{92}Kr with Z = 30, 31, 32, 33, 34, and 35, respectively, and a similar procedure is applied for the fragments of ^{90}Kr. When we compare the results with the experimental data in Figure 2, one may see that the SMM overestimates the fragment yields at the neutron-rich side of the isotopic curves. This is because the experimental isotopic yields were not fully taken into account due to the filters used during the measurements. On the other hand, it is seen that the predicted curves are located under the experimental ones at the proton-rich side. Even though the reason is not clearly known, we believe that it may stem from the model approximations and nuclear structure effects. Towards the multifragmentation region of intermediate mass fragments (IMF) with $3 \leq Z \leq 30$, we show the results in Figure 3 for the lighter fragments with Z = 29–26 emitted from the ensemble sources of ^{92}Kr. One may see a satisfactory agreement of the SMM calculations with the experimental results in this figure, when comparing to Figure 2. This means that the SMM code describes the neutron rich fragments well when the nucleon exchange reactions are considered at

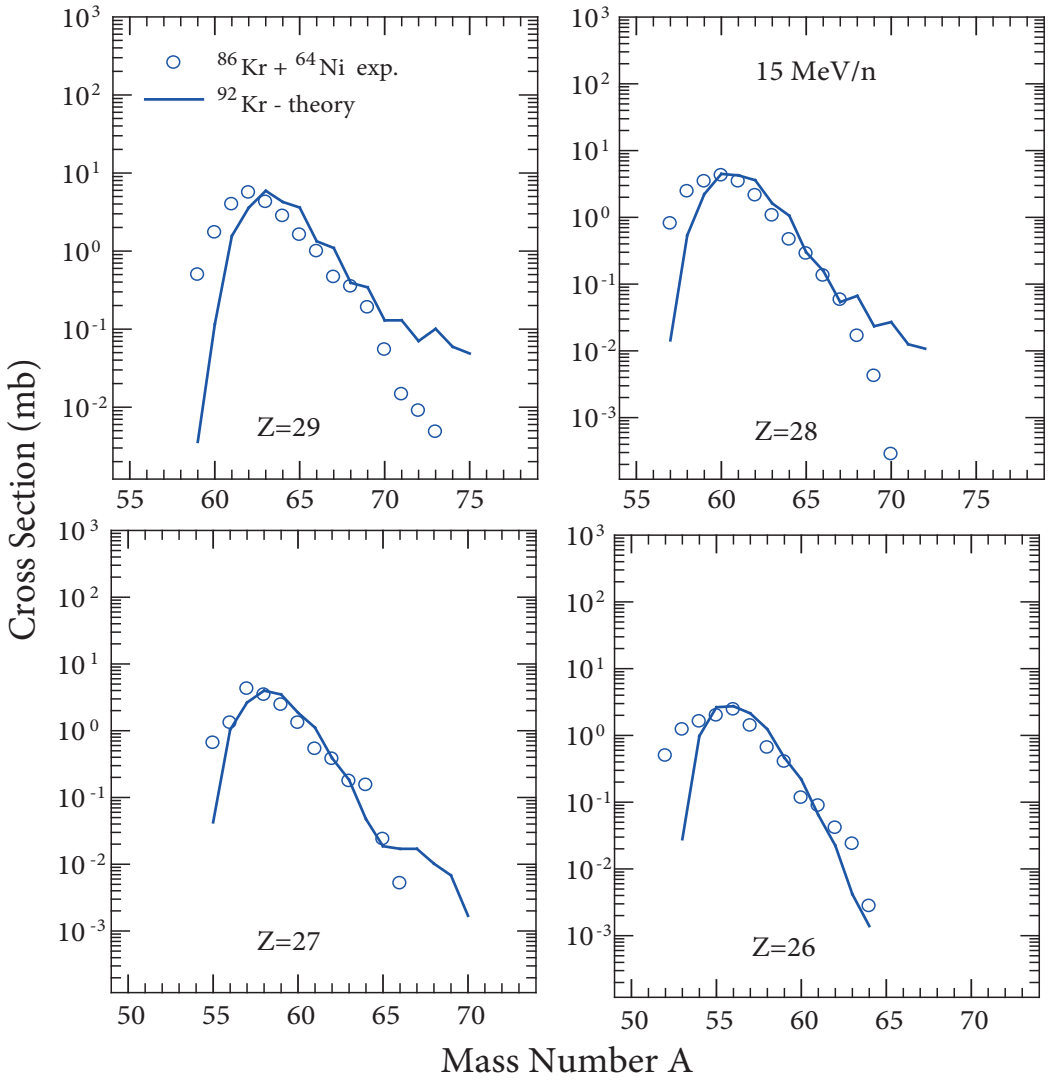

Figure 3. Isotopic distributions of projectile fragments in multifragmentation regime (there are at least 3 fragments with Z > 2) with Z = 29–26 produced from the ensemble sources of ^{92}Kr quasiprojectiles assumed to be formed through the deep inelastic neutron transfer in the reactions ^{86}Kr +^{64}Ni at 15 MeV/nucleon. The empty circles show experimental data and solid lines the present ensemble calculations.

the dynamical stage. We did not include our results for lighter fragments with Z $<$ 26, since we do not have the experimental data for these fragments to make a comparison. However, one can see the multifragmentation products emitted from the reactions ^{86}Kr $+^{58,64}$Ni at 15 MeV/n from the scatter plots of experimental data up to Z = 20 in Ref. [12].

4. Discussion and conclusions

We analyzed the reactions ^{86}Kr $+^{64}$Ni and ^{86}Kr + ^{58}Ni at 15 MeV/nucleon on the basis of the SMM. It is clear from the comparison with the experimental data that SMM ensemble calculations combined with multinucleon transfer models may reproduce the experimental data even at low energies between the Coulomb barrier and Fermi energy regime. However, one may observe from Figure 2 that SMM predictions show apparent overestimations of isotopic yields at the neutron-rich side. This is simply due to filtering the measurements during the experiments. It is also observed from the same figure that neutron-rich projectiles give rise to production of more neutron-rich isotopes as a result of the neutron transfer to the excited projectiles. Therefore, one may need additional approximations assumed to be combined with the SMM, such as stochastic nucleon transfer models, which may offer a good description of the transfer reactions near the Coulomb barrier. On the other hand, in our recent analyses we investigated the effect of the neutron richness of target nuclei on the projectile fragments and found that there was not a considerable influence of targets in projectile fragmentation reactions at relativistic [14,15,33], and Fermi energies [29–31]. However, in the present analysis we have noticed that the significant effect of the target on the neutron richness of the produced isotopes near Coulomb barriers should be taken into account. Therefore, it was a good fit to take into account the possibility of multinucleon transfer in the first step of the dynamical stage at the beginning of the reaction on the basis of deep inelastic transfer.

Consequently, it is possible to produce neutron-rich isotopes towards the neutron dripline in nucleon exchange reactions near the Coulomb barrier, as was shown experimentally in various studies [12,34]. Detailed experimental data are needed to extract information for the properties of neutron-rich exotic nuclei towards neutron dripline in nuclear charts. This will also provide us with very useful tools for investigating the stellar matter properties at extreme conditions [35,36].

Acknowledgment

We would like to thank Professors AS Botvina and W Trautmann for fruitful collaborations and helpful discussions.

References

[1] Casten, R. F.; Sherrill, B. M. *Prog. Part. Nucl. Phys.* **2000**, *45*, 171-233.

[2] Sneden, C.; Cowan, J. J. *Science* **2003**, *299*, 70-75.

[3] Botvina, A. S.; Mishustin, I. N. *Phys. Rev. C* **2001**, *63*, 061601(R).

[4] Buyukcizmeci, N.; Botvina, A. S.; Mishustin, I. N.; Ogul, R.; Hempel, M.; Schaffner-Bielich, J.; Thielemann, F. K.; Frusawa, S.; Sumuyoshi, K.; Yamada, S. et al. *Nucl. Phys. A* **2013**, *907*, 13-54.

[5] Kelic, A.; Schmidt, K. H.; Enqvist, T.; Boudard, A.; Armbruster, P.; Benlliure, J.; Bernas, M.; Czajkowski, S.; Legrain, R.; Leray, S. et al. *Phys. Rev. C* **2004**, *70*, 064608.

[6] Geissel, H.; Armbruster, P.; Behr, K. H.; Brunle, A.; Burkard, K.; Chen, M.; Folger, H.; Franczak, B.; Keller, H.; Klepper, O. et al. *Nucl. Instr. Meth. B* **1992**, *70*, 286-297.

[7] Devaraja, H. M.; Heinz, S.; Beliuskina, O.; Comas, V.; Hofmann, S.; Hornung, C.; Münzenberg, G.; Nishio, K.; Ackermann, D.; Gambhir, Y. K. et al. *Phys. Lett. B* **2015**, *748*, 199-203.

[8] Beliuskina, O.; Heinz, S.; Zagrebaev, V.; Comas, V.; Heinz, C.; Hofmann, S.; Knöbel, R.; Stahl, M.; Ackermann, D.; Hessberger, F. P. et al. *Eur. Phys. J. A* **2014**, *50*, 161.

[9] Fountas, P. N.; Souliotis, G. A.; Veselsky M.; Bonasera, A. *Phys. Rev. C* **2014**, *90*, 064613.

[10] Barlini, S.; Piantelli, S.; Casini G.; Maurenzig, P. R.; Olmi, A.; Bini, M.; Carboni, S.; Pasquali, G.; Poggi, G.; Stefanini, A. A. et al., *Phys. Rev. C* **2013,** *87*, 054607.

[11] Ma, Y. G. *Phys. Rev. Lett.* **1999,** *83*, 3617-3620.

[12] Souliotis, G. A.; Veselsky, M.; Galanopoulos, M.; Jandel, M.; Kohley, Z.; May, L. W.; Shetty, D. V.; Stein, B. C.; Yennello, S. J. *Phys. Rev. C* **2011**, *84,* 064607.

[13] Bondorf, J. P.; Botvina, A. S.; Iljinov, A. S.; Mishustin, I. N.; Sneppen, K. *Phys. Rep.* **1995**, *257*, 133-221.

[14] Ogul, R.; Botvina, A. S.; Atav, U.; Buyukcizmeci; N.; Mishustin, I. N.; Adrich, P.; Aumann, T.; Bacri, C. O.; Barczyk, T.; Bassini, R. et al. *Phys. Rev. C* **2011**, *83*, 024608.

[15] Imal, H.; Ergun, A.; Buyukcizmeci, N.; Botvina, A. S.; Trautmann, W. *Phys. Rev. C* **2015**, *91*, 034605.

[16] Ogul, R.; Atav, U.; Bulut, F.; Buyukcizmeci, N.; Erdogan, M.; Imal, H.; Botvina, A. S.; Mishustin, I. N. *J. Phys. G: Nucl. Part. Phys.* **2009**, *36*, 115106.

[17] Buyukcizmeci, N.; Imal, H.; Ogul, R.; Botvina, A. S.; Mishustin, I. N. *J. Phys. G Nucl. Part. Phys.* **2012**, *39*, 115102.

[18] Aichelin, J.; Peilert, G.; Bohnet, A.; Rosenhauer, A.; Stocker, H.; Greiner, W. *Phys. Rev. C* **1988**, *37*, 2451-2468.

[19] Vicentini, V.; Jacucci, G.; Pandharipande, V. R. *Phys. Rev. C* **1985**, *31*, 1783-1793.

[20] Papp, G.; Nemeth J.; Bondorf, J. P. *Phys. Lett. B* **1992**, *278*, 7-10.

[21] Ogul, R. *Int. J. Mod. Phys. E* **1998**, *7*, 419-424.

[22] Botvina, A. S.; Mishustin I. N.; Begemannblaich, M.; Hubele, J.; Imme, G.; Iori, I.; Kreutz, P.; Kunde, G.; Kunze, W. D.; Lindenstruth, V. et al. *Nucl. Phys. A* **1995**, *584*, 737-756.

[23] Das Gupta, S.; Mekjian, A. Z. *Phys. Rev.* C **1998**, *57*, 1361-1365.

[24] Chaudhuri, G.; Das Gupta, S. *Phys. Rev.* C **2009**, *80*, 044609.

[25] Weisskopf, W. *Phys. Rev.* **1937**, *52*, 295-303.

[26] Botvina, A. S.; Iljinov, A. S.; Mishustin, I. N.; Bondorf, J. P.; Donangelo, R.; Sneppen, K. *Nucl. Phys. A* **1987**, *475*, 663-686.

[27] Buyukcizmeci, N.; Ogul, R.; Botvina, A. S. *Eur. Phys. J. A* **2005**, *25*, 57-64.

[28] Henzlova, D.; Botvina, A. S.; Schmidt, K. H.; Henzl, V.; Napolitani, P.; Ricciardi, M. V. *J. Phys. G* **2010**, *37*, 085010.

[29] Ergun, A.; Imal, H.; Buyukcizmeci, N.; Botvina, A. S. *Phys. Rev. C* **2015**, *92*, 014610.

[30] Buyukcizmeci, N.; Ergun, A.; Imal, H.; Ogul, R.; Botvina, A. S. *Nucl. Sci. Tech.* **2015**, *26*, S20507.

[31] Buyukcizmeci, N.; Bulut, F.; Erdogan, M.; Imal, H.; Botvina, A. S.; Mishustin, I. N.; Trautmann, W. *A. Phys. Pol. B* **2011**, *42*, 697-700.

[32] Ogul, R.; Buyukcizmeci, N.; Ergun, A.; Botvina A. S. *Nucl. Sci. Tech.* **2017**, *28*, 18.

[33] Trautmann, W.; Bianchin, S.; Botvina A. S.; Le Fevre, A.; Leifels, Y.; Sfienti, C.; Buyukcizmeci, N.; Ogul, R.; Mishustin, I. N.; Chartier, M. *Int. J. Mod. Phys. E* **2010**, *19*, 1653-1663.

[34] Corradi, L.; Pollarolo, G.; Szilner, S. *J. Phys. G* **2009**, *36*, 113101.

[35] Botvina, A. S.; Mishustin, I. N. *Nucl. Phys. A* **2010**, *843*, 98-132.

[36] Buyukcizmeci, N.; Botvina, A. S.; Mishustin, I. N.; Ogul, R.; Hempel, M.; Schaffner-Bielich, J.; Thielemann, F. K.; Furusawa, S.; Sumiyoshi, K.; Yamada, S. et al. *Nucl. Phys. A* **2013**, *907*, 13-54.